2020 IEEE/RSJ International Conference on Intelligent Robots and Systems (IROS)
October 25-29, 2020, Las Vegas, NV, USA (Virtual)

Observer-Based Disturbance Control for Small-Scale Collaborative Robotics

Ahmad Awde[1,2], Mokrane Boudaoud[2], Stéphane Régnier[2], Cédric Clévy[1]

***Abstract*— Collaborative robotics allows merging the best capabilities of humans and robots to perform complex tasks. This allows the user to interact with remote and directly inaccessible environments such as the micro-scale world. This interaction is made possible by the bidirectional exchange of information (displacement - force) between the user and the environment through a haptic interface. The effectiveness of the human/robot interaction is highly dependent on how the human feels the forces. This is a key point to enable humans to make the right decisions in a collaborative task. This paper discusses the design of a dynamic observer to estimate the forces applied by a human operator on a class of parallel pantograph-type haptic interfaces used to control small-scale robotic systems. The objective is to reject disturbances in order to improve the human force perception capability over a wide frequency range. A dynamic pantograph model is proposed and experimentally validated. The observer is designed on the basis of the proposed dynamic model and its efficiency in estimating the applied human force is demonstrated for the first time with pantograph-type interfaces. Experimental validation first shows the effectiveness of the perturbation observer for external human force estimation with a response time of less than 0.2 s and a mean error of less than 7 mN and then the effectiveness of the controller in improving the quality of human sensation of forces down to 10 mN.**

I. INTRODUCTION

Performing efficient and safe robotic tasks in the small scales ($1\ nm - 100\ \mu m$) in an automated or remotely operated manner has been one of the main challenges in recent years. Several robotic systems with high resolution, precision and flexibility are now available [1], but they are not yet intelligent enough to handle complex tasks [2]. For example, the assembly of micro-mechanical components in a watch or the assembly of integrated optical devices is often performed by a human operator, who is able to adapt his mode of operation when faced with unpredictable situations. However, the human has not the required capabilities to deal with the physics at the small scales such as feeling forces at the micro-Newton and positioning the manipulation tool with a micrometer resolution. Microrobotic systems are able to cope with such physical constraints [3] [4] [5], but they are not able to make intelligent decisions. Collaborative robotics [6] is a key technology to improve the productivity of robotic tasks at the micro-scales.

Collaboration between a human and a robot, often referred to as cobotics, is characterized by direct or indirect interaction between the human and the robot to achieve a common objective. Much work on robotics at the macro scale has shown the effectiveness of the collaborative approach to perform tasks in the industrial, military, agricultural and surgical fields [7] [8] [9] [10] [11] [12]. At the micro scale, tele-operated and automated approaches have demonstrated their efficiency and complementarity in various applications such as micro-assembly [13] [14] [15] [16] [17] and biology [18] [19]. Usually a micro-robot (e.g. a micro-positioner) with a force feeling capability is coupled to a haptic interface. It is manipulated by a human operator and allows him to feel the forces applied by the micro-robot and to control the movement of the end effector [14] [20]. One of the main problems is that the force felt by the human is not only the force proportional to that returned by the micro-robot effector, but also the undesirable inertial and frictional forces of the haptic interface as well as the disruptive forces generated by the human. For a better force feeling, these undesirable perturbations must be suppressed [21].

This paper deals with human applied force estimation and disturbance rejection for a fine force feeling over a wide frequency range. Such issue is essential for effective human decision-making in a collaborative task. In this study, we focus on the pantograph-type interface originally presented in [22] [23], whose main advantage is that it has a uniform response over the entire range of human tactile frequencies [20]. The objective is to design a disturbance observer based on a dynamic model of the pantograph. The observer aims to estimate the force applied by humans on the interface and to reject undesirable disturbances in order to better feel the forces returned by the robot's effector. Several Disturbance-Observer-Based Control (DOBC) methods have been reported in the literature [24] but none of them have been designed and experimentally validated for pantograph-type interfaces.

The remainder of this paper is organized as follows. Section II describes the architecture and purpose of a disturbance observer. The main architecture and characteristics of the pantograph studied in this article are described in section III. Pantograph modeling is presented in IV. Section V deals with the observer design by considering the dynamic model of the pantograph and the control strategy. Experimental validations are presented in sections VI and VII.

II. DISTURBANCE OBSERVER

The basic architecture of a disturbance observer is shown in Fig. 1 [24]. Such an observers is useful when the disturbance d is not measurable.

[1]Univ. Bourgogne Franche-Comté, FEMTO-ST, UFC/CNRS/ENSMM, 24 rue Savary, 25000 Besancon, FRANCE ahmad.awde,cedric.clevy@femto-st.fr

[2]Sorbonne Université, Institut des Systèmes Intelligents et de Robotique, UMR 7222, ISIR, F-75005 Paris, France ahmad.awde, mokrane.boudaoud, stephane.regnier@sorbonne-universite.fr,

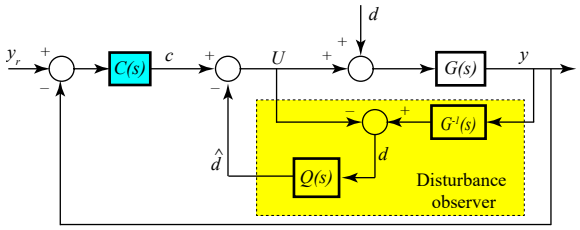

Fig. 1: Architecture of a disturbance observer used in a closed loop control scheme.

$G(s)$ is the model of the system to be controlled, U is the control input, y is the controlled output, y_r is the input reference, $C(s)$ is the transfer function of the controller, $Q(s)$ is the transfer function of a filter, d is the input disturbance and $\hat{d}$ is the estimated disturbance at the output of the observer. The filter $Q(s)$ is mainly designed to ensure that the transfer function $Q(s)G(s)^{-1}$ is implementable, i.e. the order of the numerator is less or equal to that of the denominator. It is often a low-pass filer for which the cutoff frequency must be chosen to ensure that $\hat{d} = d$ in the frequency bandwidth of interest. In this paper, the focus is not on feedback control using $C(s)$ but mainly on the observer design for the estimation of the human force applied on the pantograph.

III. Pantograph

The pantograph is shown in Fig. 2. It consists mainly of two DC brushless motors, a parallel mechanical structure and two optical encoders for measuring the rotation angles and speed of the motors. The main specifications of each component are presented in the Table I. The torques τ_1 and τ_4 generated at active joints 1 and 4 (Fig. 3) are translated into forces $F_m = \begin{bmatrix} F_{mx} & F_{my} \end{bmatrix}$ at the point E . At this point, the human operator applies and feels the forces. By applying a force $F_h = \begin{bmatrix} F_{hx} & F_{hy} \end{bmatrix}$, the end effector moves and its position is tracked by measuring the rotation angles of joints 1 and 4.

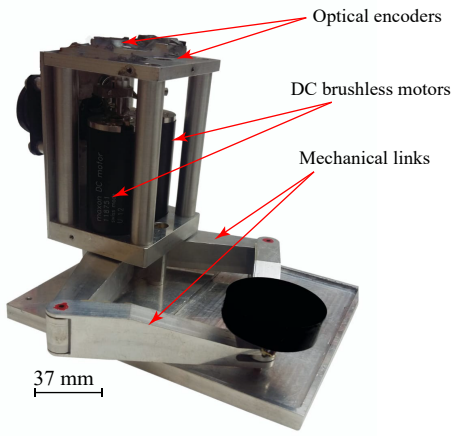

Fig. 2: Pantograph interface at ISIR lab.

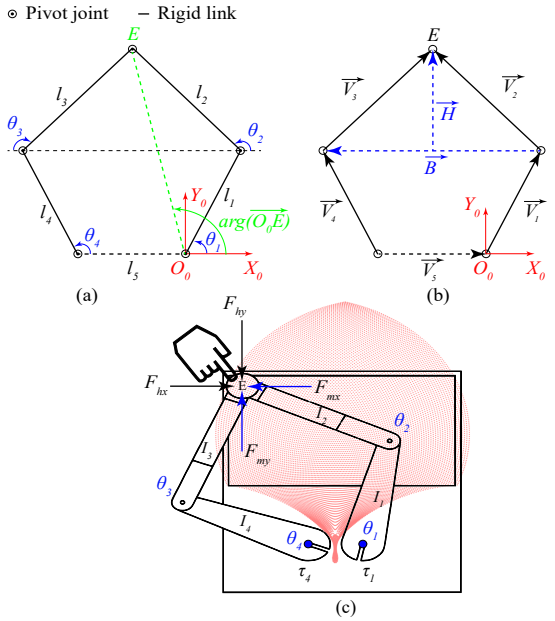

Fig. 3: Geometric representation of the pantograph: (a) dimensions, (b) vectors representation and (c) human/interface interaction forces representation at point E. F_h: human applied force. F_m: interface applied force without the inertia effect.

IV. Kinematic and Dynamic Modeling

A. Kinematic Modeling

The problem is to find the coordinates X_E and Y_E of the end effector E from the two measured joint angle θ_1 and θ_4 where the optical encoders are mounted (Fig. 3). The origin frame $\mathscr{F}_0 = \{O_0, X_0, Y_0\}$ is set at the first joint such as represented in Fig. 3 (b). To solve this problem, each link j is represented by a vector $\overrightarrow{V_j}$, where :

$$||\overrightarrow{V_j}|| = l_j, \quad \arg \overrightarrow{V_j} = \theta_j, \quad Z(\overrightarrow{V_j}) = l_j e^{i\theta_j},$$

l_j and θ_j, are respectively the length and the orientation angle of the link j as shown in Fig. 3 (a), where $j = 1,2,3,4,5$.

$Z(\overrightarrow{V_j})$ is the Euler representation of the complex number represented by the vector $\overrightarrow{V_j}$.

To obtain the coordinates X_E and Y_E in the base reference $\mathscr{F}_0 = \{O_0, X_0, Y_0\}$, the vector $\overrightarrow{O_0E}$ must be determined,

TABLE I: Pantograph components specifications

Component	Properties	Value
Brushless DC Motor Maxon RE 25	Power	20 W
	Nominal torque	24.2 mN.m
	Rotor inertia I_{motor}	9.11 gcm^2
	Torque constant	16.1 mN.m / A
MicroE systems Inc optical Encoder	Resolution	100000 CPR
	Max speed	8640 RPM
Mechanical linkages	5 light weight aluminium linkage	–

where:

$$\begin{aligned} Z(\overrightarrow{O_oE}) &= l_{O_0E}e^{iarg(\overrightarrow{O_oE})} \\ &= l_{O_0E}\cos\Big(\arg(\overrightarrow{O_oE})\Big) + il_{O_0E}\sin\Big(\arg(\overrightarrow{O_oE})\Big) \\ &= X_E + iY_E \end{aligned} \tag{1}$$

l_{O_0E} and $arg(\overrightarrow{O_oE})$ are respectively the length and the angle of orientation of $\overrightarrow{O_0E}$.

Considering Fig. 3 (b) and taking into account the fact that $||\overrightarrow{V}_2||$ and $||\overrightarrow{V}_3||$ are equal (because $l_2 = l_3$), $\overrightarrow{O_0E}$ is calculated by a summation of vectors:

$$\begin{aligned} \overrightarrow{O_0E} &= \overrightarrow{V}_1 + 0.5\overrightarrow{B} + \overrightarrow{H}, \\ \overrightarrow{B} &= +\overrightarrow{V}_4 - \overrightarrow{V}_5 - \overrightarrow{V}_1, \end{aligned} \tag{2}$$

The vector $\overrightarrow{H}$ is perpendicular to $\overrightarrow{B}$.

Expressing Eq. (2) with the complex representation yields to:

$$\begin{aligned} Z(\overrightarrow{O_0E}) &= Z(\overrightarrow{V}_1) + 0.5Z(\overrightarrow{B}) + Z(\overrightarrow{H}), \\ Z(\overrightarrow{B}) &= -Z(\overrightarrow{V}_4) + Z(\overrightarrow{V}_5) + Z(\overrightarrow{V}_1), \end{aligned} \tag{3}$$

With:

$$\begin{aligned} Z(\overrightarrow{V}_1) &= l_1 e^{i\theta_1}, & Z(\overrightarrow{V}_4) &= l_4 e^{i\theta_4}, \\ Z(\overrightarrow{V}_5) &= l_5, & Z(\overrightarrow{H}) &= He^{i\theta_H}, \\ H &= \sqrt{l_2^2 - (\tfrac{||\overrightarrow{B}||}{2})^2}, & \theta_H &= \arg(\overrightarrow{B}) - \tfrac{\pi}{2}, \end{aligned} \tag{4}$$

Finally, from Eq. (4) and (3):

$$\begin{aligned} Z(\overrightarrow{O_0E}) &= 0.5(l_1 e^{i\theta_1} - l_5 + l_4 e^{i\theta_4}) + He^{i\theta_H} \\ X_E &= \text{Real}(Z(\overrightarrow{O_0E})), Y_E = \text{Img}(Z(\overrightarrow{O_0E})) \end{aligned} \tag{5}$$

The Jacobian matrix can be found by a direct differentiation of the end effector E coordinates with respect to the actuated joints θ_1 and θ_4:

$$J = \begin{bmatrix} \frac{\partial X_E}{\partial \theta_1} & \frac{\partial X_E}{\partial \theta_4} \\ \frac{\partial Y_E}{\partial \theta_1} & \frac{\partial Y_E}{\partial \theta_4} \end{bmatrix}, \tag{6}$$

Eq. (6) can be used to map the joint-space torques onto the task-space forces as follows [25]:

$$F_m = J^{T^{-1}}\tau_m, \tag{7}$$

where $\tau_m = \begin{bmatrix}\tau_1 & \tau_4\end{bmatrix}^T$ is the input torque vector presented in the joint space and $F_m = \begin{bmatrix}F_{mx} & F_{my}\end{bmatrix}^T$ is the force applied by the interface on the contact point E resulting from the torques τ_1 and τ_4.

Note : the theoretical work-space of the contact point E is the red space represented in Fig. 3 . However, the real workspace is limited to the rectangular surface where the human operator can move the point E. In this rectangular space, the singularity of the jacobian matrix is avoided.

B. Dynamic Modeling

To obtain the dynamic equation of motion, the Euler-lagrange method based on Fig. 3 (c) is used:

$$\frac{\partial}{\partial t}\left(\frac{\partial T}{\partial \dot{q}}\right) - \frac{\partial T}{\partial q} = Q \tag{8}$$

where T is the total energies of the system, q is the state variable vector $q = [\theta_1 \;\; \theta_2 \;\; \theta_3 \;\; \theta_4]^T$ and Q is the total torque acting on the system including the pantograph motor input torque τ_m and the external human torque τ_h.

The pantograph is a planar mechanism, the total energies is only the summation of the kinetic energies T_i of each link, $i = 1 \ldots 4$.

$$T = \sum_{i=1}^{4} T_i \tag{9}$$

As shown in Fig. 3 (c), the links 1 and 4 have rotational motion only whereas the links 2 and 3 undergoes translational and rotational motion. Therefore, the kinetic energies can be described as follows:

$$\begin{aligned} T_1 &= 0.5(I_1 + I_{motor})\dot{\theta}_1^2, \\ T_2 &= 0.5I_2\dot{\theta}_2^2 + \frac{m_2}{2}(l_1^2\dot{\theta}_1^2 + c_2^2\dot{\theta}_2^2 + l_1c_2\dot{\theta}_1\dot{\theta}_2 r_{21}), \\ T_3 &= 0.5I_3\dot{\theta}_3^2 + \frac{m_3}{2}(l_4^2\dot{\theta}_4^2 + c_3^2\dot{\theta}_3^2 + l_4c_3\dot{\theta}_4\dot{\theta}_3 r_{54}), \\ T_4 &= 0.5(I_4 + I_{motor})\dot{\theta}_4^2, \end{aligned} \tag{10}$$

$r_{21} = \cos(\theta_2 - \theta_1)$ and $r_{54} = \cos(\theta_4 - \theta_3)$.

where m_i and I_i are respectively the mass and the moment of inertia of a link i. In addition, c_i is the distance between the center of mass of a link i and its rotation joint.

I_{motor} is the moment of inertia of each of the pantograph motors. The parameters m_i, I_i and c_i of each link are obtained using Solidworks software.

Based on Eq. (8), the dynamic equation of the pantograph in the joint space is given by:

$$I_n(q)\ddot{q} + B_n(q,\dot{q})\dot{q} = \tau_m - \tau_h, \tag{11}$$

where $I_n(q) \in \mathbb{R}^{4\times4}$ and $B_n(q,\dot{q}) \in \mathbb{R}^{4\times4}$ are the inertia matrix and Coriolis damping matrix of the system in the joint space, respectively. Let us recall that $\tau_m = \begin{bmatrix}\tau_1 & \tau_4\end{bmatrix}^T$ and $\tau_h \in \mathbb{R}^{2\times1}$ are the pantograph motor input torque and the external human torque, respectively. $I_n(q)$ is given by:

$$I_n(q) = \begin{pmatrix} I_{11} & I_{12} & 0 & 0 \\ I_{21} & I_2 + m_2c_2^2 & 0 & 0 \\ 0 & 0 & I_3 + m_3c_3^2 & I_{34} \\ 0 & 0 & I_{43} & I_{44} \end{pmatrix}, \tag{12}$$

where:

$$\begin{aligned} I_{11} &= I_1 + I_{motor} + m_2l_1^2, & I_{12} &= I_{21} = 0.5(m_2l_1c_2r_{21}), \\ I_{44} &= I_4 + I_{motor} + m_3l_4^2\ , & I_{34} &= I_{43} = 0.5(m_3l_5c_3r_{54})\ , \end{aligned}$$

$B_n(q,\dot{q})$ is given by:

$$B_n(q,\dot{q}) = \begin{pmatrix} 2U_1\dot{\theta}_2 & -U_1\dot{\theta}_2 & 0 & 0 \\ U_1\dot{\theta}_1 & -2U_1\dot{\theta}_1 & 0 & 0 \\ 0 & 0 & 2U_2\dot{\theta}_4 & -U_2\dot{\theta}_4 \\ 0 & 0 & U_2\dot{\theta}_3 & -2U_2\dot{\theta}_3 \end{pmatrix}, \tag{13}$$

where:

$U_1 = 0.5(m_2l_1c_2\sin(\theta_2 - \theta_1)), U_2 = 0.5(m_3l_4c_3\sin(\theta_4 - \theta_3))$.

Therefore, we project the equation of motion onto the task-space to obtain:

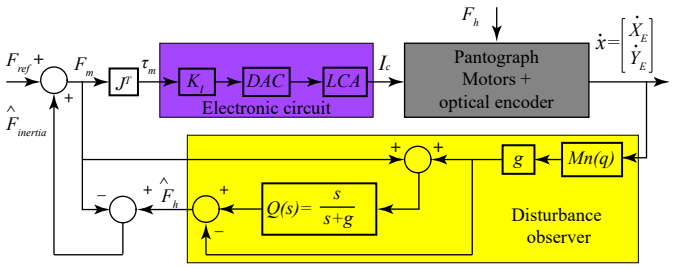

Fig. 4: Block diagram of control scheme with the disturbance observer.

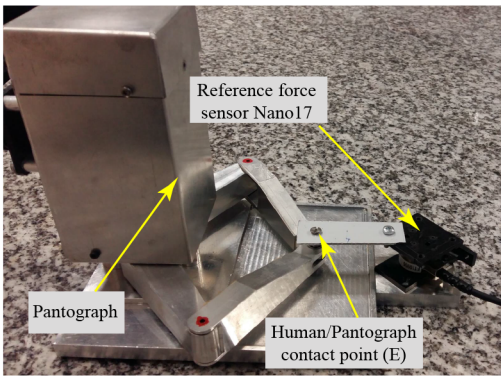

Fig. 5: Experimental setup for force measurement.

$$M_n(q)\ddot{x}+C_n(q,\dot{q})\dot{x}=F_m-F_h, \tag{14}$$

where $x=\begin{bmatrix}X_E & Y_E\end{bmatrix}^T$. In addition, $M_n(q)\in\mathbb{R}^{2\times2}$ and $C_n(q,\dot{q})\in\mathbb{R}^{2\times2}$ are the inertia and Coriolis damping matrices of the system expressed in the task-space.

These matrices can be expressed as follows [26]:

$$\begin{aligned} M_n(q)&=\mathbb{J}^{-T}I_n(q)\mathbb{J}^{-1},\\ C_n(q,\dot{q})&=\mathbb{J}^{-T}B_n(q)\mathbb{J}^{-1}-M_n(q)\dot{\mathbb{J}}\mathbb{J}^{-1}, \end{aligned} \tag{15}$$

Where $\mathbb{J}^{-1}\in\mathbb{R}^{4\times2}$ is the pseudo inverse of the Jacobian matrix $\mathbb{J}\in\mathbb{R}^{2\times4}$ defined as:

$$\mathbb{J}=\begin{bmatrix}\frac{\partial X_E}{\partial\theta_1} & 0 & 0 & \frac{\partial X_E}{\partial\theta_4}\\ \frac{\partial Y_E}{\partial\theta_1} & 0 & 0 & \frac{\partial Y_E}{\partial\theta_4}\end{bmatrix}. \tag{16}$$

In the pantograph, the force $C_n(q,\dot{q})\dot{x}$ is negligible compared to $M_n(q)\ddot{x}$. Therefore, the equation (14) is simplified as follows:

$$M_n(q)\ddot{x}=F_m-F_h, \tag{17}$$

In the sequel, an observer based on the scheme of Fig. 1 will be designed to estimate the disturbance F_h. The matrix $M_n(q)$ will be used as an internal model for the observer design.

V. Disturbance Observer Design for the Pantograph

From equation (17), the force F_h applied by the human on the point E of the pantograph (Fig.3 (c)) is:

$$\begin{aligned} F_h&=F_m-F_{inertia},\\ F_{inertia}&=M_n(q)\ddot{x}, \end{aligned} \tag{18}$$

Let us consider F_{ref} a desired reference force that the human has to feel at the point E. The aim is that the human feels the force F_{ref} without the effect of the pantograph inertia, i.e. $F_h=F_{ref}=F_m-F_{inertia}$. From Eq. (18), in static mode, $\ddot{x}=0$, the human senses only the force F_m. In dynamic mode, the influence of the inertia force $F_{inertia}=M_n(q)\ddot{x}$ appears in the human force feeling.

Therefore, the main idea is to consider F_h as a disturbance to be estimated and to use the estimated signal $\hat{F}_h$ in order to cancel $F_{inertia}$ so that the human feels only F_{ref}, i.e. $F_h=F_{ref}$. Fig. 4 shows the control block diagram of the pantograph to improve the human feeling. The force F_m is translated into torques through the Jacobian matrix. The current I_C needed to ensure the torque control is obtained through the torque constant of the motors K_I. Initially I_C was a digital current that has been converted into an analog current using a Digital to Analog Converter (DAC) and a Linear Power Amplifier (LCA). The disturbance F_h can be estimated through the observer whose inputs are F_m and $\dot{x}$.

The observer equation is described as follows:

$$\hat{F}_h=(Q(s)(F_m+g\times M_n(q)\dot{x}))-g\times M_n(q)\dot{x} \tag{19}$$

where $Q(s)=\frac{g}{s+g}$ is a low pass filer with a cut of frequency $\omega_c=g=540$ rad/s that is selected large enough to cover the dynamic frequency range of pantograph movement.

Proof of the observer:

$$\begin{aligned} \hat{F}_h&=[Q(s)(F_m+gM_n(q)\dot{x})]-gM_n(q)\dot{x}\\ &=Q(s)F_m+Q(s)gM_n(q)\dot{x}-gM_n(q)\dot{x}\\ &=Q(s)F_m+(Q(s)-1)gM_n(q)\dot{x}\\ &=(\frac{g}{s+g})\times(F_m-M_n(q)s\dot{x})\\ &=(\frac{g}{s+g})\times(F_m-M_n(q)\ddot{x})\\ &=(\frac{g}{s+g})\times(F_m-F_{inertia})\\ &=(\frac{g}{s+g})\times F_h \end{aligned} \tag{20}$$

Therefore, $\hat{F}_h$ is a filtered estimation of F_h.

With such a scheme, one can obtain (Fig. 4):

$$\begin{aligned} F_m&=F_{ref}+\hat{F}_{inertia}\\ &=F_{ref}+F_m-F_h \end{aligned} \tag{21}$$

Hence: $F_{ref}=F_h$.

VI. Experimental Validation

The control scheme of Fig. 4 is designed using Matlab/Simulink and is implemented through a dSPACE controller board.

A. Force Generation

The aim here is to demonstrate that the reference force F_{ref} signal defined at the input of the control scheme of Fig. 4 is faithfully applied on the point E of the pantograph (Fig. 3 (c)). A Nano17 (SI-120.12) force sensor is used to measure

the force F_{my} in y direction generated by the pantograph at the point E as shown in Fig. 3 (c). The experimental setup for the validation procedure is shown in Fig. 5. The block diagram of Fig. 4 is used to control the pantograph.

The results are represented in Fig. 6. Based on these results, the pantograph can generate desired reference forces at the point E with an error less than 7 mN and a response time $\approx 0.1s$. This validation is of importance because it first shows the effectiveness of the pantograph model that is used in Fig. 4 and it demonstrates that the force felt by the human at the point E will be the force F_{ref} when the inertia force is cancelled.

B. Observer Validation

The aim here is to evaluate the effectiveness of the observer for the estimation of the human force F_h. For that purpose, the force feedback $\hat{F}_{inertia}$ is not considered, i.e. $F_m = F_{ref}$

The idea here is to consider that when the point E of the pantograph is free, i.e. no interaction with a human, for a constant reference force F_{ref}, the output of the observer $\hat{F}_h$ must tends towards 0 when the time $t \to \infty$.

Different values of F_{ref} are applied to the pantograph, namely 0.01 N, 0.05 N and 0.1 N without the presence of the human operator on the pantograph interface. Three signals are considered: F_{ref} generated by the user, $\hat{F}_h$ obtained at the output of the observer and $F_{inertia}$ deduced from Eq. (18) that allows to consider $F_{inertia} = F_{ref} - \hat{F}_h$ since $F_m = F_{ref}$ in these experiments. Experimental results are shown in Fig. 7. The estimated human force $\hat{F}_h$ always tends towards 0 in steady state which validate the expectations and therefore validate the observer experimentally. For the best knowledge of the authors, this is the first time that the human force estimation is validated experimentally for pantograph type structures.

Note that $F_{inertia}$ is always the inverse of $\hat{F}_h$ with an offset due to F_{ref}.

C. Human Force Feeling

The aim here is to analyze experimentally how the human force feeling is improved with the control scheme of Fig. 4 using the observer and the force feedback $\hat{F}_{inertia}$. Without loss of generality, the experiments are performed considering x axis. The same results can be observed when considering y axis.

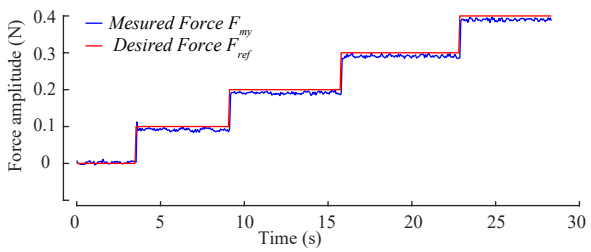

Fig. 6: Experimental measurements of the generated force by the pantograph F_{my} at the point E.

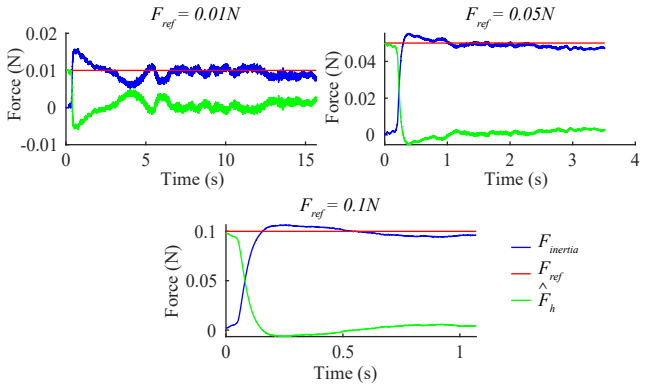

Fig. 7: Measurements of F_{ref}, $\hat{F}_h$ and $F_{inertia}$ for the validation of the observer.

The experiments are performed as follows. A constant reference force F_{ref}= 0.1 N is defined as the input of the control scheme of Fig. 4. The human operator moves the points E of the pantograph in two ways. The first one is referred as slow motion when the human motion does not produce significant inertia forces $F_{inertia}$ from the interface. The second one is referred as fast motion when the human motion produces significant inertia forces $F_{inertia}$ from the interface.

Theses two ways of motion are of importance because the effectiveness of the control scheme of Fig. 4 and therefore the effectiveness of the fine human force feeling must be validated regardless of the way the human uses the pantograph. For each ways of motion the experiments are performed with $\hat{F}_{inertia}$ force feedback (i.e. $F_m = F_{ref} + \hat{F}_{inertia}$) and without $\hat{F}_{inertia}$ force feedback (i.e. $F_m = F_{ref}$).

For slow motion experiments, the results are shown in Fig.

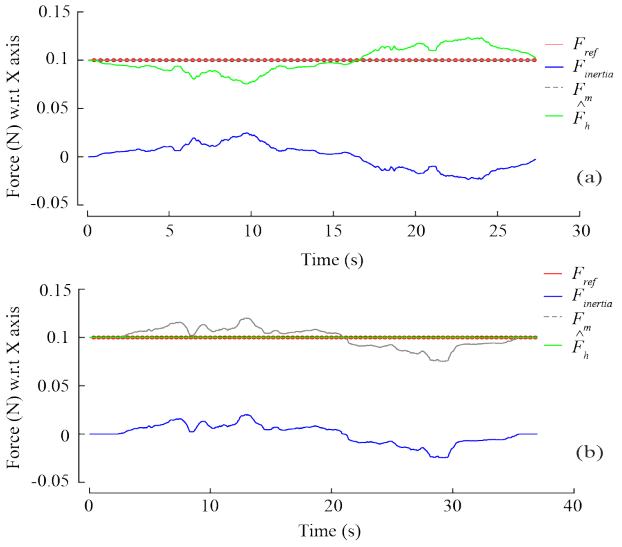

Fig. 8: Slow motion experiments. Comparison between the human force $\hat{F}_h$ and the reference force F_{ref} (a) without $\hat{F}_{inertia}$ force feedback (i.e. $F_m = F_{ref}$) and (b) with $\hat{F}_{inertia}$ force feedback (i.e. $F_m = F_{ref} + \hat{F}_{inertia}$).

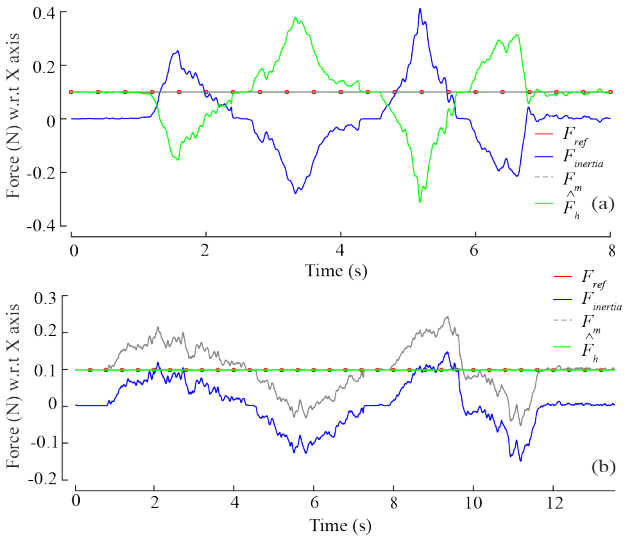

Fig. 9: Fast motion experiments. Comparison between the human force $\hat{F}_h$ and the reference force F_{ref} (a) without $\hat{F}_{inertia}$ force feedback (i.e. $F_m = F_{ref}$) and (b) with $\hat{F}_{inertia}$ force feedback (i.e. $F_m = F_{ref} + \hat{F}_{inertia}$).

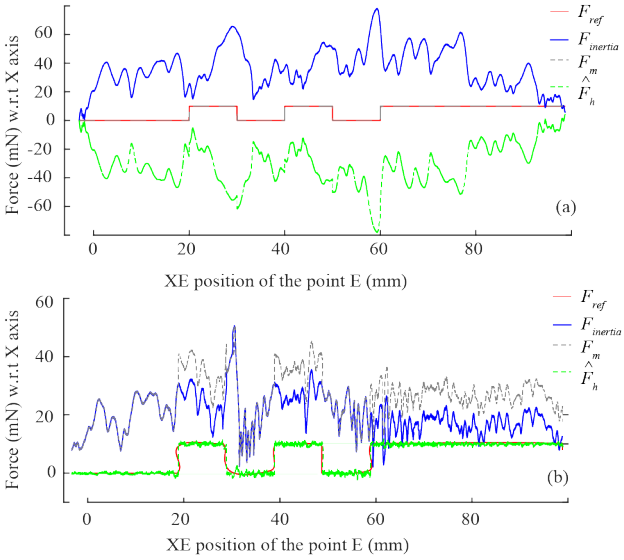

Fig. 10: Slow motion experiments. Comparison between the human force $\hat{F}_h$ and the reference force F_{ref} (a) without $\hat{F}_{inertia}$ force feedback and (b) with $\hat{F}_{inertia}$ force feedback.

8. The inertia force $\hat{F}_{inertia}$ is close to zeros. But even in this case, it affects the human feeling $\hat{F}_m$ when no force feedback is applied on the control scheme (Fig. 8 (a)). When the force feedback is applied, the human feels a force $\hat{F}_m$ that has the same amplitude as the reference force F_{ref} (Fig. 8 (b)). For fast motion experiments, the results are shown in Fig. 9. The inertia force $\hat{F}_{inertia}$ is much higher than previously. It greatly affects the human feeling $\hat{F}_m$ when no force feedback is applied on the control scheme (Fig. 9 (a)). When the force feedback is applied, the human feels a force $\hat{F}_m$ that has the same amplitude as the reference force F_{ref} (Fig. 9 (b)).

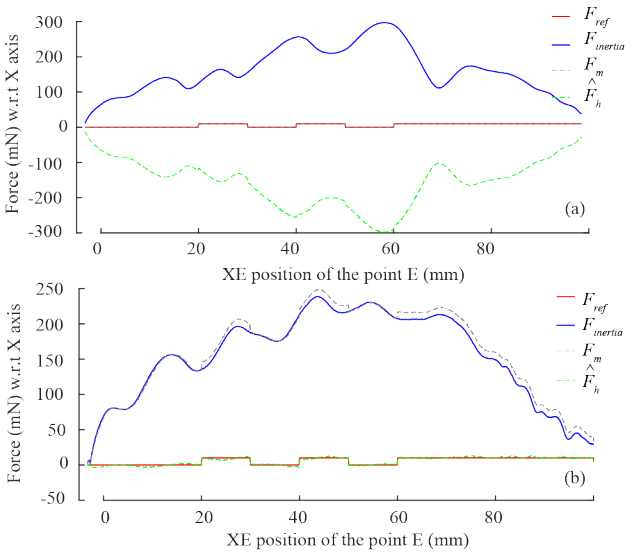

Fig. 11: Fast motion experiments. Comparison between the human force $\hat{F}_h$ and the reference force F_{ref} (a) without $\hat{F}_{inertia}$ force feedback and (b) with $\hat{F}_{inertia}$ force feedback.

These results validate the transparency of the pantograph interface with the observer design.

VII. Positioning with respect to force feeling

The perception of the human at the tip of his finger is limited to 10 mN [27]. This value varies from one operator to another and is affected by various parameters such as temperature, humidity, age, etc. In this section, we analyze the possibility of using the pantograph with the observer for force feeling at the limit of human perception.

The experiments of section VI-C have shown that the perception of force as small as $0.1\ N = 100\ mN$ is affected by the pantograph inertia force $F_{inertia}$ without force rejection, but the feeling is much better when applying inertia force rejection. Here, we analyze if the inertia force rejection with the observer is good enough to feel the limit of perception, i.e. $F_{ref} = 10\ mN$.

Therefore, the reference force F_{ref} is here generated as shown in Fig. 10 and Fig. 11 for slow motion and fast motion modes. These results clearly indicate that even with a fast motion mode, a force as small as 10 mN can be transmitted at the point E free from other perturbation forces even when the inertia force amplitude reaches 20 times the value of F_{ref} as shown in Fig. 11 (b).

VIII. Conclusions

This paper investigated the design and implementation of a disturbance observer for pantograph-type parallel haptic interfaces. The aim has been to improve the human force feeling for micro-robotic collaborative tasks. A dynamic model of the pantograph has been proposed. This model was used for the observer design. The idea was to consider the human force as a disturbance to be estimated and to use the estimated signal to cancel the inertial forces of the

pantograph so that the human feels only a desired reference force. The effectiveness of the observer in estimating applied human forces has been experimentally validated. The control structure with inertial force rejection has experimentally demonstrated the ability to detect forces as small as 10 *mN* even when the magnitude of the inertial force reaches 20 times the value of the reference force. The proposed observer design with the pantograph interface is the first step toward collaborative robotics applications at the small scales where the force feeling in dynamic motion modes is of primary importance. The main perspective of this work is to use the pantograph with the observer for collaborative micro-robotic tasks where the reference forces are provided by micro-force sensors.

ACKNOWLEDGMENT

This work was supported by the COLAMIR project (Contract "ANR-16-CE10-0009"), the Bourgogne Franche-Comté region, the EIPHI Graduate School (contract "ANR-17-EURE-0002"), and by the Robotex platform (Contract "ANR-10-EQPX-44-01").

REFERENCES

[1] M. Boudaoud, T. Lu, S. Liang, R. Oubellil, and S. Régnier, "A voltage/frequency modeling for a multi-dofs serial nanorobotic system based on piezoelectric inertial actuators," *IEEE/ASME Transactions on Mechatronics*, vol. 23, no. 6, pp. 2814–2824, 2018.

[2] J. Agnus, N. Chaillet, C. Clévy, S. Dembélé, M. Gauthier, Y. Haddab, G. Laurent, P. Lutz, N. Piat, K. Rabenorosoa, M. Rakotondrabe, and B. Tamadazte, "Robotic microassembly and micromanipulation at femto-st," *Journal of Micro-Bio Robotics*, vol. 8, no. 2, pp. 91–106, 2013.

[3] M. Boudaoud, M. G. D. Faria, Y. L. Gorrec, Y. Haddab, and P. Lutz, "An output feedback lpv control strategy of a nonlinear electrostatic microgripper through a singular implicit modeling," *Control Engineering Practice*, vol. 28, pp. 97 – 111, 2014.

[4] R. Oubellil, A. Voda, M. Boudaoud, and S. Régnier, "Mixed stepping/scanning mode control of stick-slip sem-integrated nano-robotic systems," *Sensors and Actuators A: Physical*, vol. 285, pp. 258 – 268, 2019.

[5] R. Oubellil, A. Voda, M. Boudaoud, and S. Régnier, "A 2-dof h∞ control strategy for a 3 axes robotic system operating at the nanometer scale," in *International Conference on System Theory, Control and Computing (ICSTCC)*, pp. 355–362, 2016.

[6] G. Michalos, S. Makris, N. Papakostas, D. Mourtzis, and G. Chryssolouris, "Automotive assembly technologies review: challenges and outlook for a flexible and adaptive approach," *CIRP Journal of Manufacturing Science and Technology*, vol. 2, no. 2, pp. 81 – 91, 2010.

[7] V. Francoise, A. Sahbani, and G. Morel, "A comanipulation device for orthopedic surgery that generates geometrical constraints with real-time registration on moving bones," in *International Conference on Robotics and Biomimetics*, pp. 38–43, 2011.

[8] C. P. Torterotot, M. Vitrani, P. Mozer, and G. Morel, "Ultrasound image-based comanipulation for enhanced perception of the contacts with a distal soft organ," in *International Conference on Robotics and Biomimetics*, pp. 1140–1146, 2011.

[9] X. Lamy, F. Colledani, F. Geffard, Y. Measson, and G. Morel, "Achieving efficient and stable comanipulation through adaptation to changes in human arm impedance," in *International Conference on Robotics and Automation*, pp. 265–271, 2009.

[10] J. M. Florez, J. Szewczyk, and G. Morel, "An impedance control strategy for a hand-held instrument to compensate for physiological motion," in *International Conference on Robotics and Automation*, pp. 1952–1957, 2012.

[11] T. Carlson and Y. Demiris, "Collaborative control for a robotic wheelchair: evaluation of performance, attention, and workload," *Transactions on Systems, Man, and Cybernetics, Part B (Cybernetics)*, vol. 42, no. 3, pp. 876–888, 2012.

[12] J. Rehbein, T. Wrütz, D. Hotze, and R. Biesenbach, "Collaborative control with industrial robots," in *International Conference on Research and Education in Mechatronics (REM)*, pp. 1–4, 2017.

[13] A. Bolopion and S. Régnier, "A review of haptic feedback teleoperation systems for micromanipulation and microassembly," *Transactions on Automation Science and Engineering*, vol. 10, no. 3, pp. 496–502, 2013.

[14] A. Bolopion, H. Xie, D. S. Haliyo, and S. Régnier, "Haptic teleoperation for 3-d microassembly of spherical objects," *IEEE/ASME Transactions on Mechatronics*, vol. 17, no. 1, pp. 116–127, 2012.

[15] B. Komati, A. Kudryavtsev, C. Clévy, G. Laurent, B. Tamadazte, J. Agnus, and P. Lutz, "Automated robotic microassembly of flexible optical components," in *International Symposium on Assembly and Manufacturing (ISAM)*, pp. 93–98, 2016.

[16] S. Bargiel, K. Rabenorosoa, C. Clévy, C. Gorecki, and P. Lutz, "Towards micro-assembly of hybrid moems components on a reconfigurable silicon free-space micro-optical bench," *Journal of Micromechanics and Microengineering (JMM)*, vol. 20, 2010.

[17] M. Sitti and H. Hashimoto, "Two-dimensional fine particle positioning under an optical microscope using a piezoresistive cantilever as a manipulator," *journal of Micromechatronics*, vol. 1, no. 1, pp. 25–48, 2000.

[18] X. Fan, M. Sun, Z. Lin, J. Song, Q. He, L. Sun, and H. Xie, "Automated noncontact micromanipulation using magnetic swimming microrobots," *Transactions on Nanotechnology*, vol. 17, no. 4, pp. 666–669, 2018.

[19] J. Kuncová-Kallio and P. Kallio, "Lab automation in cultivation of adherent cells," *Transactions on automation science and engineering*, vol. 3, no. 2, pp. 177–186, 2006.

[20] T. Lu, C. Pacoret, D. Hériban, A. Mohand-Ousaid, S. Régnier, and V. Hayward, "Kilohertz bandwidth, dual-stage haptic device lets you touch brownian motion," *IEEE Transactions on Haptics*, vol. 10, no. 3, pp. 382–390, 2017.

[21] A. Mohand-Ousaid, G. Millet, S. Régnier, S. Haliyo, and V. Hayward, "Haptic interface transparency achieved through viscous coupling," *The International Journal of Robotics Research*, vol. 31, no. 3, pp. 319–329, 2012.

[22] V. Hayward, J. Choksi, G. Lanvin, and C. Ramstein, "Design and multi-objective optimization of a linkage for a haptic interface," in *Advances in robot kinematics and computational geometry*, pp. 359–368, 1994.

[23] A. Dufresne, O. Martial, and C. Ramstein, "Multimodal user interface system for blind and "visually occupied" users: Ergonomic evaluation of the haptic and auditive dimensions," in *Human—Computer Interaction*, pp. 163–168, 1995.

[24] W. Chen, J. Yang, L. Guo, and S. Li, "Disturbance-observer-based control and related methods—an overview," *Transactions on Industrial Electronics*, vol. 63, no. 2, pp. 1083–1095, 2015.

[25] O. Khatib, "A unified approach for motion and force control of robot manipulators: The operational space formulation," *Journal on Robotics and Automation*, vol. 3, no. 1, pp. 43–53, 1987.

[26] B. Siciliano, L. Sciavicco, L. Villani, and G. Oriolo, *Robotics: modelling, planning and control*. Springer Science & Business Media, 2010.

[27] G. Millet, S. Haliyo, S. Régnier, and V. Hayward, "The ultimate haptic device: First step," in *World Haptics EuroHaptics conference and Symposium on Haptic Interfaces for Virtual Environment and Teleoperator Systems*, pp. 273–278, 2009.